Decomposition-Based Assembly Synthesis of a Three-Dimensional Body-in-White Model for Structural Stiffness

Naesung Lyu
e-mail: nlyu@umich.edu

Kazuhiro Saitou[1]
e-mail: kazu@umich.edu

Department of Mechanical Engineering,
University of Michigan,
Ann Arbor, MI 48109-2125

This paper presents an extension of our previous work on decomposition-based assembly synthesis for structural stiffness, where the three-dimensional finite element model of a vehicle body-in-white (BIW) is optimally decomposed into a set of components considering (1) stiffness of the assembled structure under given loading conditions, (2) manufacturability, and (3) assembleability of components. Two case studies, each focusing on the decomposition of a different portion of a BIW, are discussed. In the first case study, the side frame is decomposed for the minimum distortion of front door frame geometry under global bending. In the second case study, the side/floor frame and floor panels are decomposed for the minimum floor deflections under global bending. In each case study, multiobjective genetic algorithm with graph-based crossover, combined with finite element methods analyses, is used to obtain Pareto optimal solutions. Representative designs are selected from the Pareto front and trade-offs among stiffness, manufacturability, and assembleability are discussed. [DOI: 10.1115/1.1799551]

1 Introduction

Complex structural products such as automotive bodies are made of hundreds of components joined together. While a monolithic design is ideal from a structural viewpoint, it is virtually impossible to economically manufacture complex structures as one piece, requiring them to be assemblies of smaller sized components with simpler geometry. Therefore, during the conceptual design stage designers need to decide a set of components by decomposing the overall product geometry of the whole structure. In industry, a handful of basic decomposition schemes considering geometry, functionality, and manufacturing issues are used. However, these decomposition schemes are usually nonsystematic and depend mainly on the designers' experience, which may cause the following problems during design and the production phases:

(i) *Problems of the insufficient assembled structure stiffness:* Components and joining methods specified by designers may not meet the desired stiffness of the assembled structure.
(ii) *Problems of manufacturability and assembleability:* Components decided by designers can not be produced or assembled in an economical way.

Since these problems are directly related to the component and/or joint configurations and therefore usually found in the production phase, solving them requires costly and time-consuming iteration procedures. Hence introducing a more systematic method of finding components set considering overall structural characteristics, manufacturability and assembleability will have a significant impact on industry.

Assembly synthesis [1,2] refers to such a systematic method where entire product geometry is decomposed into components and joints. Since joints are often structurally inferior to components, it is important that the decomposition and joint allocation are done in an optimal fashion, such that the reduction in structural performances (e.g., stiffness) is maximized while achieving economical manufacturing and assembly. As an extension of our previous work on decomposition-based assembly synthesis for structural stiffness [3], the present method optimally decomposes the three-dimensional (3D) finite element model of a vehicle body-in-white (BIW) into a set of components considering the stiffness of the assembled structure under given loading conditions, as well as the manufacturability and assembleability of components. The stiffness of the assembled structure is evaluated by finite element methods (FEM) analyses, where joints are modeled as linear torsional springs. Manufacturability of a component is evaluated as an estimated manufacturing cost based on the size and geometric complexity of components. Assuming assembly efforts are proportional to the total number of weld spots, assembleability is simply accounted for as the total rate of torsional springs. In order to allow close examination of the trade-off among stiffness, manufacturability, and assembleability, the optimization problem is solved by a multiobjective genetic algorithm [4,5], which can efficiently generate a well-spread Pareto [6,7] front over multiple objectives. A graph-based crossover scheme is adopted for the improved convergence of the algorithm.

2 Related Work

2.1 Design for Assembly/Manufacturing. Design for assembly (DFA) and design for manufacturing (DFM) refers to design methodologies to improve product and process during the design phase of a product, thereby ensuring the ease of assembly and manufacturing. Boothroyd and Dewhurst [8] are widely regarded as major contributors in the establishment of DFA/DFM theories. In their work [9], assembly costs are first reduced by the reduction of part count, followed by the local design changes of the remaining parts to enhance their assembleability and manufacturability. One of the main functions of DFA/DFM is manufacturability analysis of the product design, e.g., by evaluating the capability of production within the specified requirements such as low production costs and short production time. In general, manufacturability analysis requires a product to be decomposed into features containing a manufacturing meaning, such as, surfaces, dimensions, tolerances, and their correlations [10].

While existing DFA/DFM methods share the idea of simultaneous engineering with the present approach, they analyze or improve existing designs from the viewpoint of assembly and manu-

[1]Author to whom correspondence should be addressed.

Contributed by the Design Automation Committee for publication in the JOURNAL OF MECHANICAL DESIGN. Manuscript received July, 2003; revised March, 2004. Associate Editor: K. K. Choi.

facturing by modifying geometry of given (i.e., already decomposed) components. On the other hand, the decomposed-based assembly synthesis method presented in this paper starts with no prescribed components and generates the optimized components set considering assembleability, manufacturability, and structural characteristic of the assembled structure.

2.2 Automotive Body Structure Modeling. In automotive body design, high stiffness is one of the most important design factors since it is directly related with the improved ride and NVH (noise, vibration, and harshness) qualities and crash worthiness [11]. Therefore evaluating the structural characteristics of a vehicle, including stiffness, became a crucial factor in designing a vehicle. Before mathematical modeling techniques were not available, structural analysis was usually carried out only for the stresses in specific hardware items, such as door hinges, drive train and suspension components. Overall structural behavior could not be predicted until a vehicle prototype was built and tested. Therefore, any changes recommended from the test results were bound to be costly to implement [12]. Prior to the use of finite element methods in the automotive body analysis in the middle of the 1960s, preliminary structural analysis was performed by simple structural surface method (SSS method) [13,14], where the actual vehicle geometry was replaced with an equivalent boxlike structure composed of shear panels and reinforcing beams. With SSS methods, designers can identify the type of loading condition that is applied to each of the main structural members of a vehicle and also the nominal magnitudes of the loads to be determined based on the static conditions with load path in the structure. However, this method can be used only to the simplified conceptual design and it cannot be used to solve for loads on redundant structures with more than one load path [14].

The availability of high-powered computers, user-oriented FEM codes and economical solution methods enabled full-scale finite element vehicle models in the early 1970s. To predict the stiffness of a body structure with the finite element model more accurately, Chang [15] modeled joints as torsional springs, and demonstrated that the model can accurately predict the global deformation of automotive body substructures. Garro and Vullo [16] analyzed the dynamic behavior of typical body joints under two typical actual loading conditions. They addressed that the plates along spot welds tend to detach from each other when joint deformations occur. Lee and Nikolaidis [17] proposed a two-dimensional (2D) joint model to consider joint flexibility, offset of rotation centers, and coupling effects between the movements of joint branches. Recently, correlation between torsional spring properties of joints and the length of the structural member was studied to assess the accuracy of the joint model [18]. Long [19] studied the method of correlating the performance targets for a design of individual joints in the automotive to design variables that specify the geometry of the joint design. Kim et al. [20] employed an 8-DOF beam theory for modeling joints to consider the warping and distortion in vibration analysis.

These works, however, mainly focus on the accurate prediction of the structural behavior of a given (i.e., already ''decomposed'') assembly and individual joint design. They do not concern the selection of optimal joint locations and properties, which is addressed in the present method.

2.3 Multiobjective Optimization Algorithm. Engineering problems generally involve multiple objectives. Among the techniques to solve multiobjective optimization problems, evolutionary algorithms that simulate the natural evolution process have shown to be effective in many engineering problems [21]. The major advantages of evolutionary algorithms in solving multiobjective optimization problems are (1) they can obtain Pareto optimal solutions in a single run, and (2) they do not require derivatives of objective functions. Many evolutionary multiobjective optimization algorithms (MOGA [22], NSGA [23], NSGA-II [24], and NPGA [25]) were developed based on the two ideas suggested by Goldberg [26]: Pareto dominance and niching. Pareto dominance is used to exploit the search space in the direction of the Pareto front. Niching technique explores the search space along the front to keep diversity. Another important operator that has been shown to improve the performance of multiobjective algorithm is elitism, which maintains the knowledge of the previous generations by conserving the individuals with best fitness in the population or in an auxiliary population (SPEA [27] and PAES [28]).

Considering a proven efficiency and simplicity of NSGA-II, the present work utilizes an implementation based on NSGA-II with Pareto ranking selection.

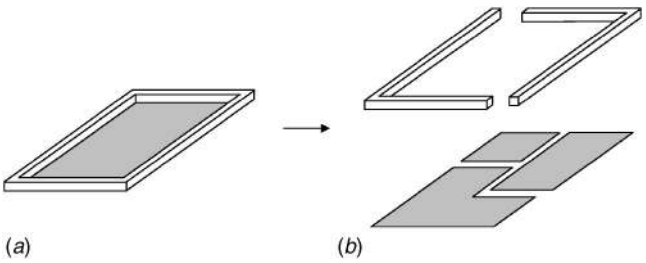

Fig. 1 (*a*) A simple structure with a plate reinforced by a beam, and (*b*) decomposition with two beam and three plate components

3 Approach

The decomposition-based assembly synthesis method simultaneously identifies the optimal components set and joint attributes considering the stiffness of the assembled structure. It consists of the following two major steps:

(1) A 3D finite element model is transformed to a structural topology graph representing the liaisons between basic members, the smallest decomposable components of the given structure, specified by the designer.
(2) The product topology graph is automatically decomposed, through an optimization process, to a set of subgraphs representing components connected together by edges representing joints.

Detailed procedure covered throughout this section uses a simple structural model composed of a plate with reinforcing beam frame shown in Fig. 1. This type of structure is widely used in automotive and aerospace industries.

3.1 Overview

Step 1: Construction of Structural Topology Graph. An entire structure is divided into substructures, each of which can be manufactured by a single process (Figs. 2(*b*) and 2(*c*)). This prevents the synthesis of the components that cannot be manufactured with a single process. Then, basic members are defined in each substructure (Figs. 2(*d*) and 2(*e*)) by the designer. In this example, four basic members (B0–B3) are defined in the beam substructure and six basic members (P0–P5) are defined in the plate substructure. Since components are represented as a group of basic members, the definition of basic member determines the diversity and resolution of the resulting components.

Then, structural topology graph $G=(V,E)$ is constructed such that

(1) a basic member m_i is represented as a node n_i in set V;
(2) the connections (liaisons) between two basic members m_i and m_j are represented as edge $e=\{n_i,n_j\}$ in set E.

As illustrated in Fig. 3, structural topology graph G_B (Fig. 3(*b*)) of the beam substructure with four nodes ($n_{B0}-n_{B3}$) and four edges ($e_{B0}-e_{B3}$) is constructed based on the basic members of

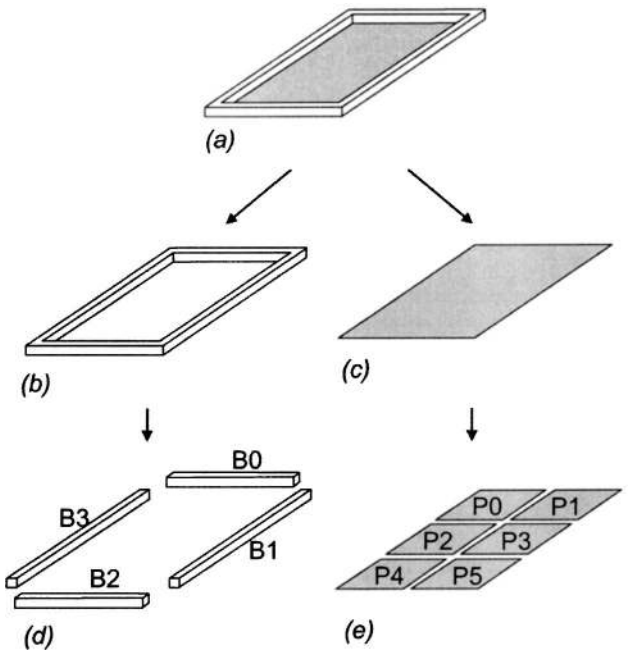

Fig. 2 (*a*) Overall structure, (*b*) beam substructure, and (*c*) plate substructure separated from (*a*), (*d*) four basic members (B0–B3) defined in (*b*), and (*e*) six basic members (P0–P5) defined in (*c*)

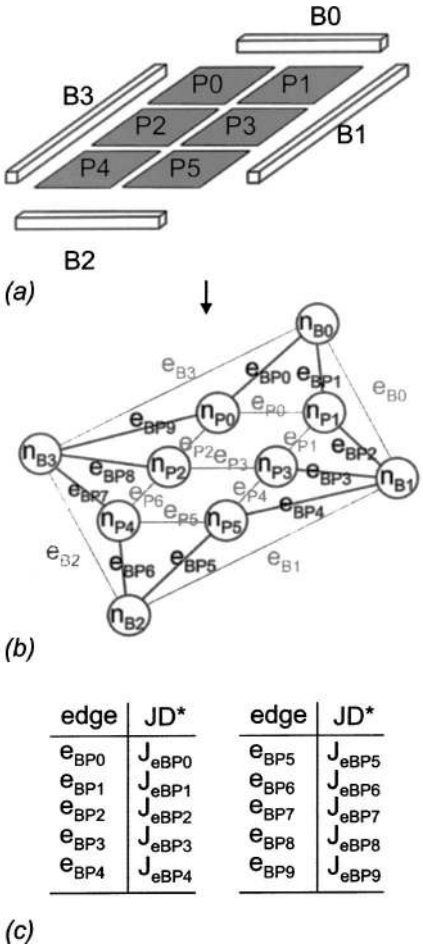

Fig. 4 (*a*) Beam and plate basic members, (*b*) entire structural topology graph G_E, and (*c*) joint designs between beam and plate basic members [thick edges in (*b*)]

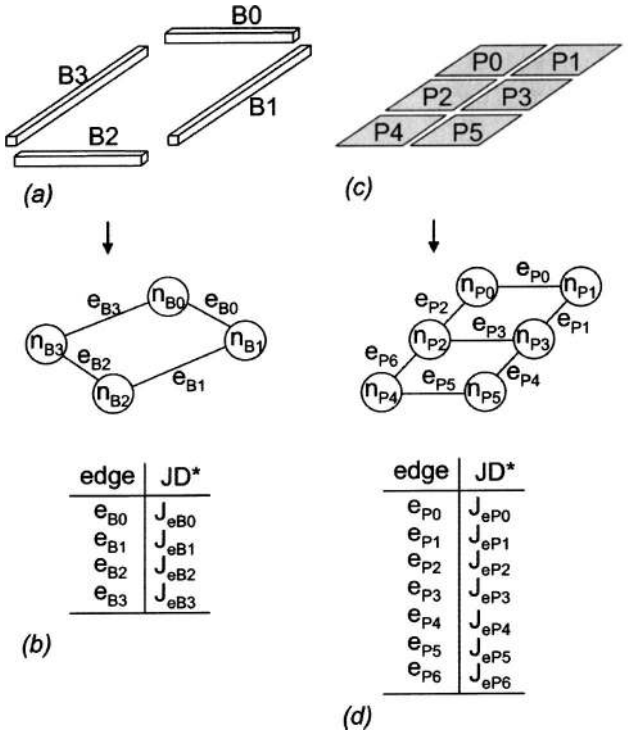

Fig. 3 Constructing structural topology graph for each substructure. (*a*) Basic members of beam substructure, (*b*) structural topology graph G_B of (*a*), (*c*) basic members of plate substructure, and (*d*) topology graph G_P of (*c*). In (*b*) and (*d*), JD* represents the joint design at each potential joint position defined for each edge.

Fig. 3(*a*). Similarly, structural topology graph G_P (Fig. 3(*d*)) of the plate substructure with six nodes (n_{P0}–n_{P5}) and seven edges (e_{P0}–e_{P6}) is constructed from the basic members in Fig. 3(*c*). Joints can occur at each connection between basic members. Hence, joint designs (JD), attributes of joints, are assigned to every edge in G_B and G_P (tables in Figs. 3(*b*) and 3(*d*)). In addition, the entire structural topology graph G_E is defined to represent the joints between substructures. In Fig. 4, joint designs between the beam and plate components (Fig. 4(*c*)) are assigned to 10 edges between the beam and plate basic members (e_{BP0}–e_{BP9}) shown as thick edges in Fig. 4(*b*).

Step 2: Decomposition of Structural Topology Graph. Components set and joint designs between the components can be decided by choosing which edges will be removed in the structural topology graphs and by assigning appropriate joint designs at the location of removed edges. The joint designs are simply assigned to all joints between substructures (edges of entire structural topology graph G_E) since they must be always present. In Fig. 5(*a*), edge e_{B1} and e_{B3} are chosen to be removed (shown in dotted lines) and the original G_B is decomposed into two subgraphs corresponding to the two beam components in Fig. 5(*b*). Note that only joint design J_{eB1} and J_{eB3} are realized in Fig. 5(*b*) because edge e_{B1} and e_{B3} are removed and therefore joints are needed to connect components. The other joint designs (J_{eB0} and J_{eB1}) colored in gray in the table indicate that they are not realized. Similarly, by removing four edges (e_{P0}, e_{P2}, e_{P3}, and e_{P4})

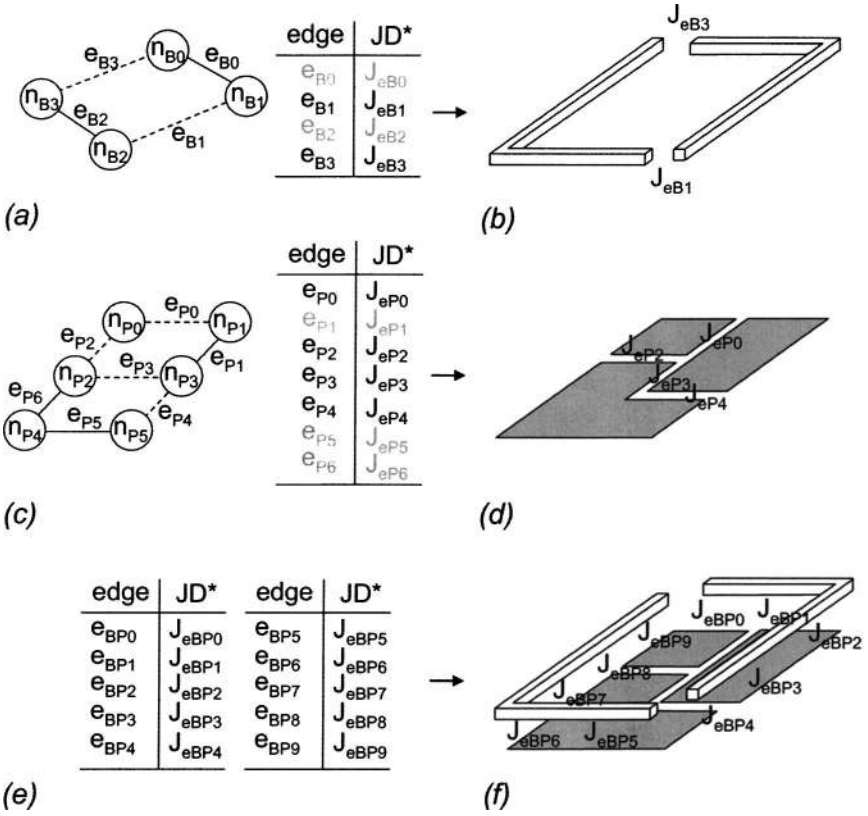

Fig. 5 Sample decomposition of structural topology graph of (*a*) beam substructure and (*b*) corresponding components set with joint designs, of (*c*) plate substructure and (*d*) corresponding components set with joint designs, (*e*) assignment of joint properties between beam and plate components, and (*f*) resulting component set

G_P is decomposed into three subgraphs corresponding to the three plate components in Fig. 5(*d*) with four joint designs (J_{eP0}, J_{eP2}, J_{eP3}, and J_{eP4}) realized.

The quality of the component set and JDs are evaluated according to the following three objectives within an optimization loop:

(1) *Stiffness of the assembled structure under given loading conditions:* it is evaluated as a displacement at a specific location of the assembled structure, calculated by FE analyses. To automatically generate FE models with joints during optimization, the default FE model that contains models for basic members (for example, Figs. 3(*a*) and 3(*c*)) is built. Then, by checking the modified structural topology graphs, basic members are connected using rigid FE elements (if the corresponding edge is present) or joint FE models (if the corresponding edge is removed) of the specified joint designs. In the following case studies, every joining is assumed to be done with spot welds, and entire joint portion is modeled as a set of torsional springs in FE analysis.

(2) *Manufacturability of components:* it is evaluated considering the total cost of producing components in the structure represented by decomposed product topology graphs G_B and G_P. The proposed method of selecting components can directly provide designers with geometry of each component. Therefore this method is (1) mostly applicable in the situations where cost of manufacturing given components is closely correlated with geometry of components and (2) providing method of checking if components are feasible for given manufacturing process. For example, extrusion process cannot produce loop-shape components. Because a loop-shape component is usually represented by a cyclic graph in the decomposed product topology graphs, designers can easily check topology graphs and avoid those infeasible components by applying high penalty cost to those components. In the following case studies, it is assumed that components are made from sheet metal working, whose cost is estimated as the cost of stamping/blanking dies. In practice, die cost is usually represented as a function of die usable area Au. For each component, Au is approximated as the area of its convex hull. A larger component results in a higher value of Au, requiring larger die set with higher cost.

(3) *Assembleability of components*: it is calculated considering the cost of assembly procedure. Cost of assembly procedures can be calculated from (1) the geometric information of components defined by the decomposed product topology graphs and/or (2) joint attributes used to join components. Since the cost of spot welding, which was used as a method of joining components in the following case studies, is proportional to the number of weld spots in the structure, and the number of weld spots in a joint is approximately proportional to the torsional stiffness of the joint, the welding cost is estimated by the sum of the rates of torsional springs (Nm/rad) in the FE model of the assembled structure.

3.2 Mathematical Formulation

Definition of Design Variables. A set of components and joint designs between the components can be defined by selecting edges to be removed in the two topology graphs (G_B and G_P) and by assigning joint designs at the location of removed edges. There are five design variables.

(1) $\mathbf{x}_B$, decomposition vector for G_B;
(2) $\mathbf{x}_P$, decomposition vector for G_P;

(3) $\mathbf{y}_B$, joint design vector for joints between beam components;
(4) $\mathbf{y}_P$, joint design vector for joints between plate components;
(5) $\mathbf{y}_{BP}$, joint design vector for joints between beam and plate components.

Decomposition vector for G_B, $\mathbf{x}_B$ represents the nonexistence of a joint (i.e., the existence of a solid connection) at each connection of two basic members (an edge in the structural topology graph) in a structure represented by G_B,

$$\mathbf{x}_B=(x_{B0},x_{B1},\ldots,x_{Bi},\ldots,x_{BnB-1}), \tag{1}$$

where $nB=|E_B|$ and

$$x_{Bi}=\begin{cases}0 & \text{if edge } e_{Bi} \text{ is removed in } G_B,\\ 1 & \text{otherwise.}\end{cases} \tag{2}$$

Decomposition vector for G_P, $\mathbf{x}_P$ is similarly defined, by replacing the subscript B with P.

Joint design vectors $\mathbf{y}_B$ represents the joint designs between beam two components:

$$\mathbf{y}_B=(\mathbf{y}_{B0},\mathbf{y}_{B1},\ldots,\mathbf{y}_{Bi},\ldots,\mathbf{y}_{BnB-1}) \tag{3}$$

Elements of vector $\mathbf{y}_B$ are in turn defined as vector $\mathbf{y}_{Bi}=(y_{Bi0},y_{Bi1},\ldots,y_{Bij},\ldots,y_{Bin-1})\in\mathbf{F}_B$, which represents J_{eBi} (joint design corresponding to ith edge e_{Bi} in G_B) from the feasible beam joint design set $\mathbf{F}_B$. Since joints are modeled as torsional springs, joint design $\mathbf{y}_{Bi}$ represents a vector of the torsional springs rates (Nm/rad). For 3D, a joint requires three design variables (rotations around spring x, y, and z-axes) and $\mathbf{y}_{Bi}=(y_{Bi0},y_{Bi1},y_{Bi2})=(k_{ix},k_{iy},k_{iz})$. However, joint attribute $\mathbf{y}_{Bi}$ is considered only when ith edge e_{Bi} is removed in G_B. Joint design vector $\mathbf{y}_P$ for plate components is similarly defined, by replacing the subscript B with P.

Element of vector $\mathbf{y}_{BP}$ is also defined similarly, by replacing subscript B with BP. However, unlike the previous $\mathbf{y}_{Bi}$ and $\mathbf{y}_{Pi}$, every joint attribute J_{eBPi} is considered and realized in the FE model. The reason is because it is assumed that there always exist a joint between beam component and plate components (in other words, beam and plate cannot form one component together).

After optimization, designers will have the optimized joint attributes for each joint. To realize a joint with these attributes, designers can use a data base of existing joints with attributes and select a real joint design from this data base that has most close attributes to those of the optimized result.

Definition of Objective Functions. A multicomponent structure represented by two decomposition vectors $\mathbf{x}_B$ and $\mathbf{x}_P$ and three joint design vectors $\mathbf{y}_B$, $\mathbf{y}_P$, and $\mathbf{y}_{BP}$ is evaluated according to the following three objectives: (1) stiffness of the assembled structure under given loading conditions, (2) manufacturability of components, and (3) assembleability of components.

The first objective function, $f_{\text{stiffness}}$, evaluates stiffness (to be maximized) of the assembled structure. Stiffness of the structure can be measured as the negative of the displacement at predefined points in the structure:

$$f_{\text{stiffness}}=-\text{DISPLACEMENTS}(G_B(\mathbf{x}_B),G_P(\mathbf{x}_P),\mathbf{y}_B,\mathbf{y}_P,\mathbf{y}_{BP}) \tag{4}$$

where DISPLACEMENTS( ) is a function that returns the total displacements at predefined points of the FE model defined by the decomposed $G_B(\mathbf{x}_B)$, $G_P(\mathbf{x}_P)$, and three joint design vectors $\mathbf{y}_B$, $\mathbf{y}_P$, and $\mathbf{y}_{BP}$.

The second objective function, f_{manufac}, evaluates manufacturability (to be maximized) of the set of components considering the total cost of producing components in the structure represented by the decomposed $G_B(\mathbf{x}_B)$ and $G_P(\mathbf{x}_P)$. As stated before, components are assumed to be made from sheet metals working, whose cost is estimated as the cost of stamping and blanking dies. The following equation is used to calculate manufacturability of a structure:

$$f_{\text{manufac}}=-\left\{\sum_{i=1}^{nBC}\text{DIECOST}_B(Au(\text{COMP}_B(i,G_B(\mathbf{x}_B))))+\sum_{j=1}^{nPC}\text{DIECOST}_P(Au(\text{COMP}_P(j,G_P(\mathbf{x}_P))))\right\}, \tag{5}$$

where $\text{COMP}_B(i,G_B(\mathbf{x}_B))$ and $\text{COMP}_P(j,G_P(\mathbf{x}_P))$ return the ith component of beam structure defined by the decomposed $G_B(\mathbf{x}_B)$ and the jth component of plate structure defined by the decomposed $G_P(\mathbf{x}_P)$, respectively. $Au(C)$ is a function that returns the die useable area of a component C. $\text{DIECOST}_B(A)$ and $\text{DIECOST}_P(A)$ are the functions that calculate the die cost with given die useable area A for beam component and plated component, respectively. Finally, nBC and nPC are the numbers of the beam and plate components in the decomposed beam and plate substructures, respectively. Hence, f_{manufac} is considered as the negative sum of die cost for all components defined by two decomposition vector $\mathbf{x}_B$ and $\mathbf{x}_P$.

The third objective function, f_{assemble}, calculates assembleability (to be maximized) of the components. In this paper, assembleability is evaluated considering cost of assembly procedure, which is assumed to be spot welding. Since the cost of spot welding for a structure is proportional to the number of weld spots in the structure, and the number of weld spots in a joint is ap-

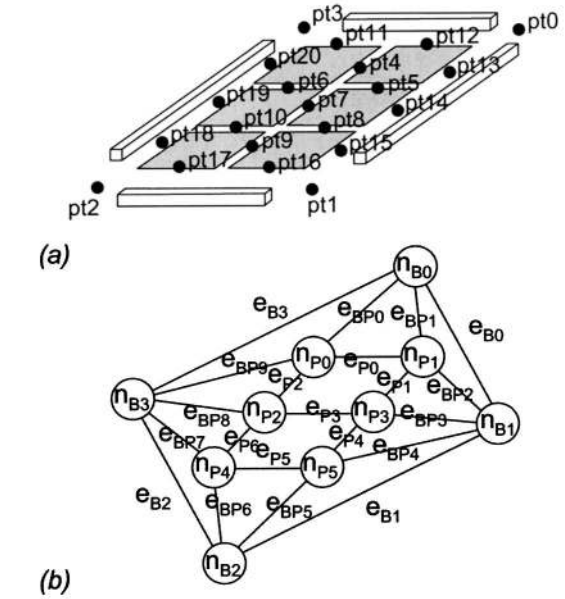

edge	pt
e_{B0}	pt0
e_{B1}	pt1
e_{B2}	pt2
e_{B3}	pt3

edge	pt
e_{P0}	pt4
e_{P1}	pt5
e_{P2}	pt6
e_{P3}	pt7
e_{P4}	pt8
e_{P5}	pt9
e_{P6}	pt10

edge	pt
e_{BP0}	pt11
e_{BP1}	pt12
e_{BP2}	pt13
e_{BP3}	pt14
e_{BP4}	pt15

edge	pt
e_{BP5}	pt16
e_{BP6}	pt17
e_{BP7}	pt18
e_{BP8}	pt19
e_{BP9}	pt20

(c)

Fig. 6 (*a*) Physical location of joints. (*b*) Entire structural graph G_E. (*c*) Table of joint points and corresponding edges in G_E.

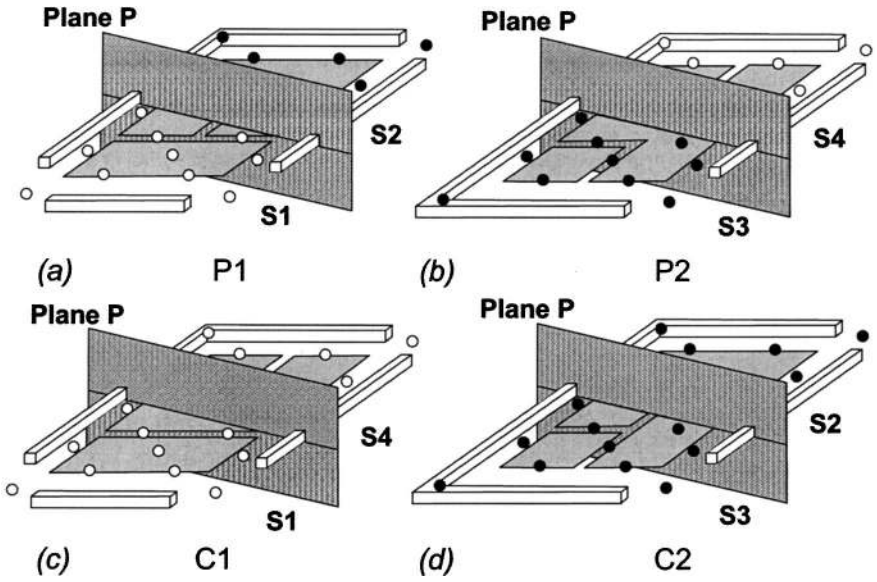

Fig. 7 "Graph-based" crossover operation by plane A. (*a*) Parent structures P1 cut into S1/S2, (*b*) another parent structure P2 cut into S3/S4, (*c*) child C1 made of S1/S4, and (*d*) child C2 made of S3/S2.

proximately proportional to the torsional stiffness of the joint, the welding cost is estimated by the sum of the rates of torsional springs (Nm/rad) in the FE model of the structure:

$$f_{\text{assemble}} = -\text{SPRINGRATE}(G_B(\mathbf{x}_B), G_P(\mathbf{x}_P), \mathbf{y}_B, \mathbf{y}_P, \mathbf{y}_{BP}). \tag{6}$$

In the above equation, SPRINGRATE is the sum of the spring rates in FE model defined by the decomposed $G_B(\mathbf{x}_B)$, $G_P(\mathbf{x}_P)$, and three joint design vectors $\mathbf{y}_B$, $\mathbf{y}_P$, and $\mathbf{y}_{BP}$.

Formulation of Optimization Problem. The design variables and the objective functions defined in the previous sections provide the following multiobjective optimization problem:

$$\text{maximize,} \quad \{f_{\text{stiffness}}, f_{\text{manufac}}, f_{\text{assemble}}\}$$

subject to

$$\mathbf{x}_B \in \{0,1\}^{|E_B|}, \quad \mathbf{x}_P \in \{0,1\}^{|E_P|},$$

$$\mathbf{y}_B \in \mathbf{F}_B^{|E_B|}, \quad \mathbf{y}_P \in \mathbf{F}_P^{|E_P|},$$

$$\mathbf{y}_{BP} \in \mathbf{F}_{BP}^{|E_{BP}|}.$$

Note that there is no explicit constraint in this problem.

3.3 Optimization Algorithm. Due to the complexity of the underlying graph partitioning problem [29] and the multiobjective formulation without predefined weight or bounds on the objective functions, the above optimization problem is solved using a modified Non-Dominated Sorting Genetic Algorithm II (NSGA-II) [24]. This algorithm uses the nondominated sorting method for Pareto ranking procedure, which successfully applied in our previous study [30].

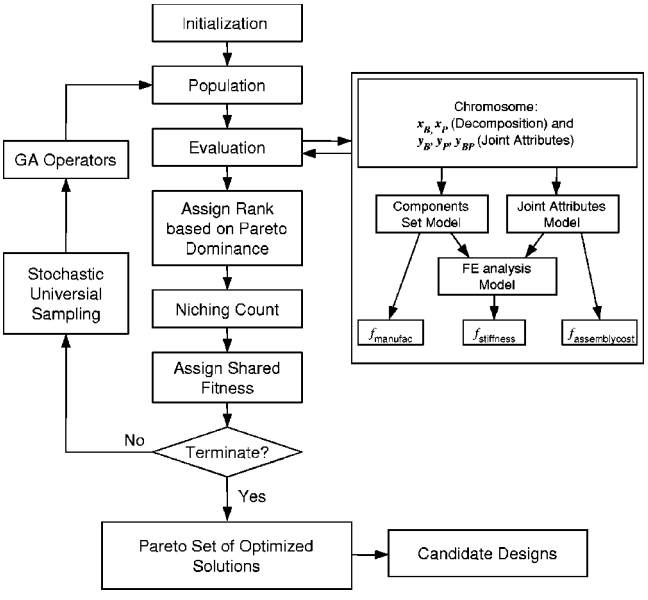

Fig. 8 Flowchart of multicomponent structure synthesis

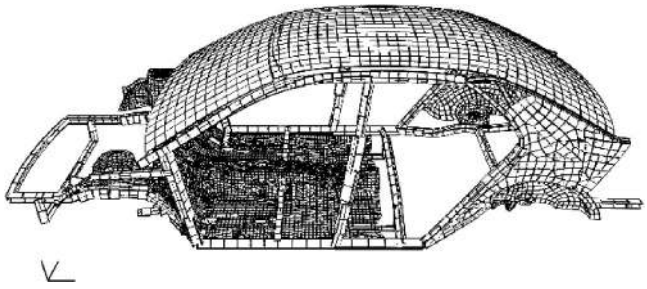

Fig. 9 FE model of a four door passenger vehicle BIW composed of beam and plate elements

Table 1 Properties of BIW model used in case studies I and II

Properties	Count
DOF	108 672
GRID	20 507
CBEAM	597
CQUAD4	15 788
CTRIA3	1160

Table 2 Parameter values of GA in case studies I and II

Properties	Value
Maximum # of generation	100
Number of population	300
Replacement rate (m/n)	0.5
Crossover probability	0.9
Mutation probability	0.10

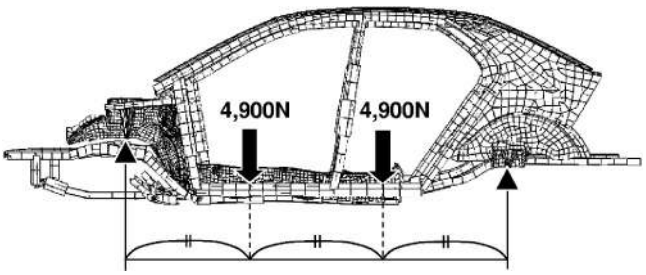

Fig. 10 Global bending condition used for case studies I and II. Two downward loads of 4900 [N] (1/4 of total weight) are applied at nodes on the rocker at the 1/3 distance between the supports.

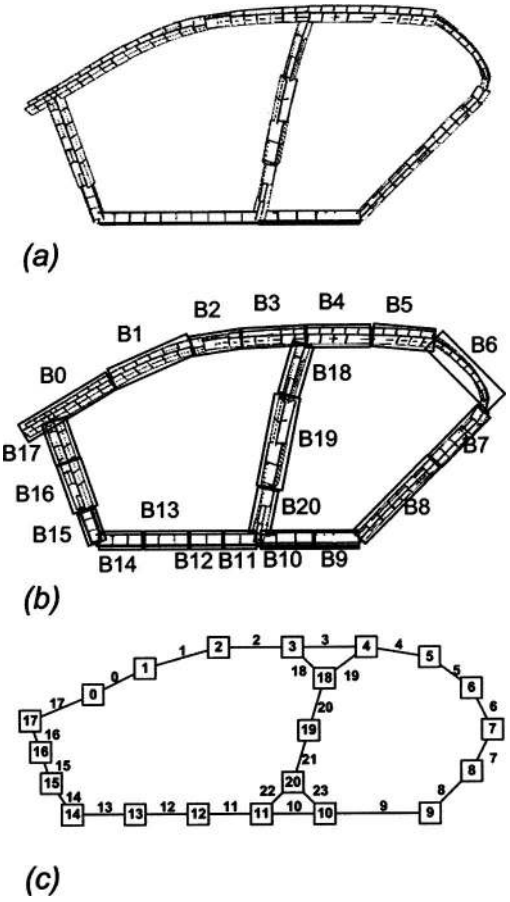

Fig. 11 (*a*) Side frame portion of the FE model made of beam elements, (*b*) selected 21 basic members, and (*c*) corresponding entire structural topology graph G_E with 21 nodes and 24 edges

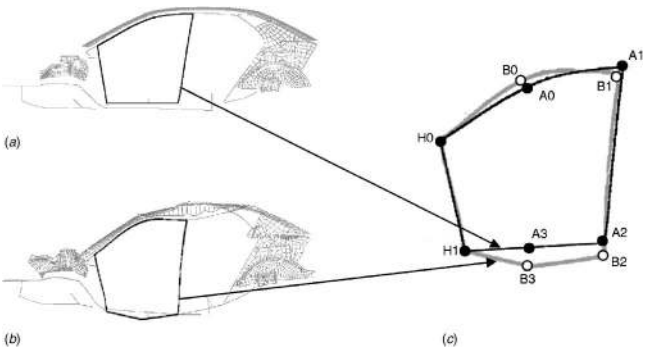

Fig. 12 (*a*) Side frame before deformation and (*b*) after deformation, and (*c*) calculation of front door frame distortion. Black line, front door shape in (*a*) and gray line, front door shape in (*b*). DISPLACEMENTS will be the maximum distance between *Ai* and *Bi* (*i*=0,1,2,3).

A chromosome **c** (an internal representation of design variables for GA) is simply a list of the five design variables:

$$\mathbf{c}=(\mathbf{x}_B,\mathbf{x}_P,\mathbf{y}_B,\mathbf{y}_P,\mathbf{y}_{BP}). \tag{7}$$

Since information in the decomposition vectors ($\mathbf{x}_B$ and $\mathbf{x}_P$) and joint design vectors ($\mathbf{y}_B$, $\mathbf{y}_P$, and $\mathbf{y}_{BP}$) are linked in a nonlinear fashion, the conventional one point or multiple point crossover for linear chromosomes [26] does not effectively preserve high-quality partial solutions (building blocks). For this type of problem, graph-based crossover has been successfully applied for improved performance of GA [6,7,30], which is modified to fit the current problem as described below:

(1) Find the joint points which represent the physical locations of joints in two parent structures P1 and P2 (Fig. 6).
(2) Create an arbitrary plane A that "cut" the set of joint points of P1 into S1 and S2, and the set of joint points of P2 into S3 and S4 (Figs. 7(*a*) and 7(*b*)).

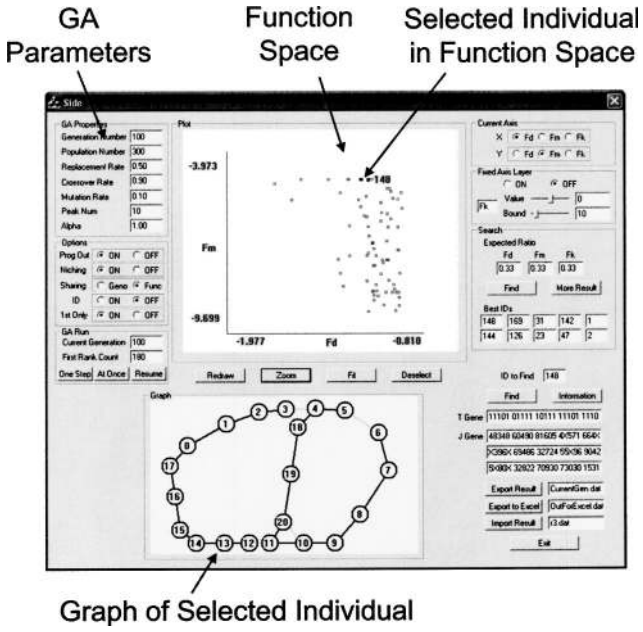

Fig. 13 GUI of the optimization software used in case study I

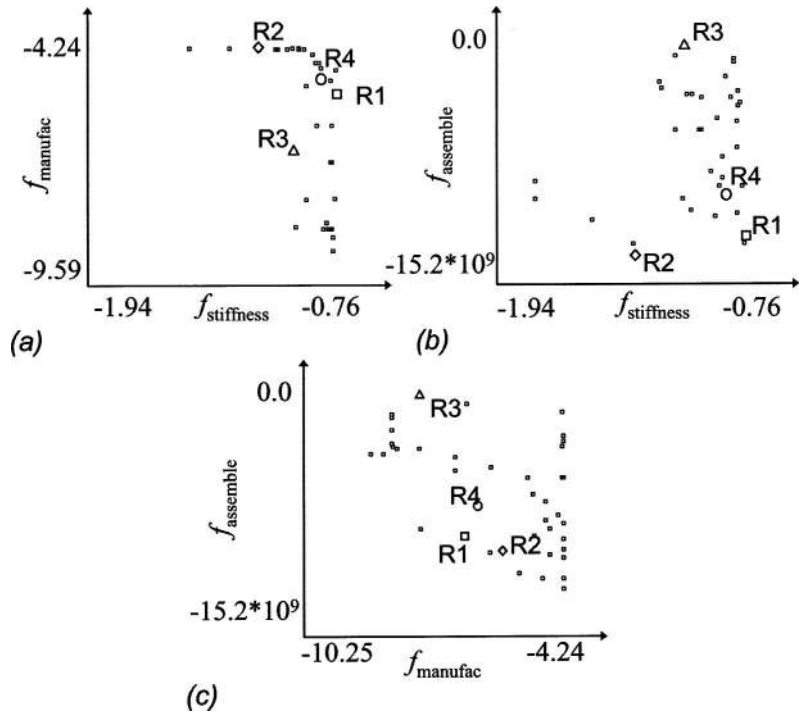

Fig. 14 Function values at the terminal generation (generation number=100). Points in the plots are the Pareto optimal designs.

(3) Construct two child structures C1 and C2 by "swapping" S2 and S4 (Figs. 7(*c*) and 7(*d*)) based on the decomposition and joint design of the parents.

In addition to the above custom crossover, the implementation of NSGA-II used in this paper utilizes linear fitness scaling, niching based on the distances in objective function space, and stochastic universal sampling. Figure 8 shows the flowchart of the optimization. Software implementation, including NSGA-II code, is done in the C++ programming language. LEDA library was used for graph algorithm and commercial FEM software, MSC NASTRAN is used to obtain $f_{stiffness}$.

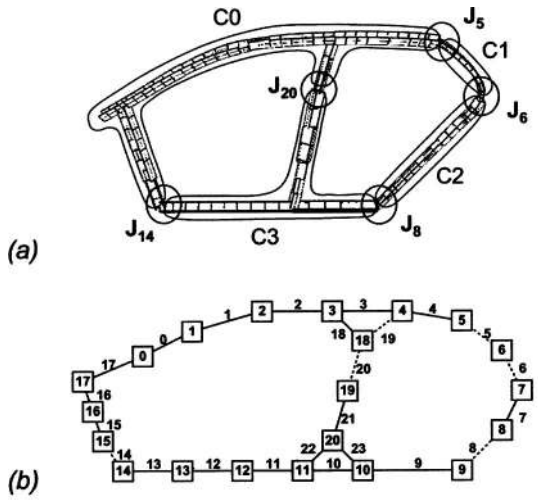

JD	k_x	k_y	k_z
J_5	0.8	0.001	0.3
J_6	1.0	0.001	0.3
J_8	0.5	0.2	0.2
J_{14}	0.5	0.6	0.6
J_{20}	0.7	0.001	0.7

*unit of k_x, k_y, k_z: [10^9 Nm/rad]

(c)

Fig. 15 Design R1 (best $f_{stiffness}$). (*a*) Four components, (*b*) structural topology graph, and (*c*) joint designs.

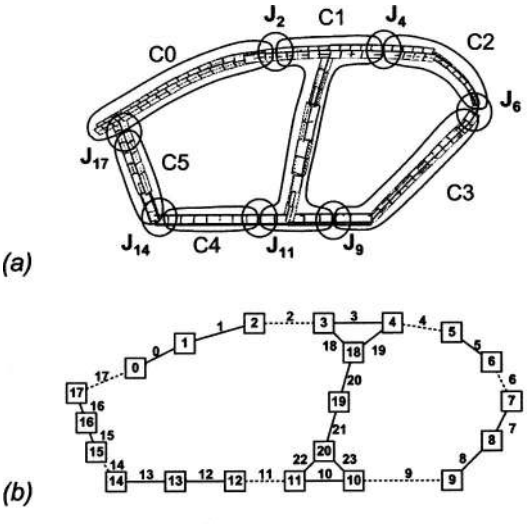

JD	k_x	k_y	k_z
J_2	0.3	0.001	0.9
J_4	0.4	0.2	0.1
J_6	0.1	0.5	0.1
J_9	0.2	0.001	0.4
J_{11}	0.001	0.2	0.4
J_{14}	0.1	0.5	0.7
J_{17}	0.4	0.9	0.7

*unit of k_x, k_y, k_z: [10^9 Nm/rad]

(c)

Fig. 16 Design R2 (best $f_{manufac}$). (*a*) Five components (*b*) structural topology graph, and (*c*) joint designs.

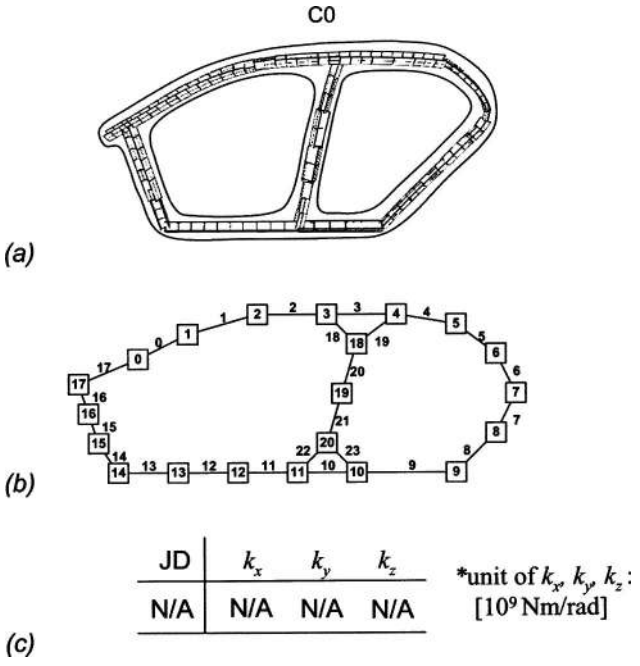

Fig. 17 Design R3 (best $f_{assemble}$). (*a*) One component, (*b*) structural topology graph, and (*c*) joint designs: not available (no joints).

4 Case Studies

Two case studies are discussed in this section. In the first case study, the side frame of a FE model of a four door passenger vehicle BIW (Fig. 9 and Table 1) is decomposed for the minimum distortion of front door geometry under global bending. In the second case study, the side frame and floor panels of the same FE model are simultaneously decomposed for the minimum floor deflection under global bending. The FE model is composed of beam and plate elements. Table 2 lists the parameters values for GA used in the case studies. These parameters were selected considering the convergence trend of the number of individuals in the Pareto front.

In both case studies, the following assumptions are made:

(1) Body is subject to a global bending due to the weight of the vehicle (Fig. 10).
(2) Components are symmetric in the left and right sides of the body.
(3) Components are joined with joints with spot welds. Each joint is modeled as three torsional springs whose axes of

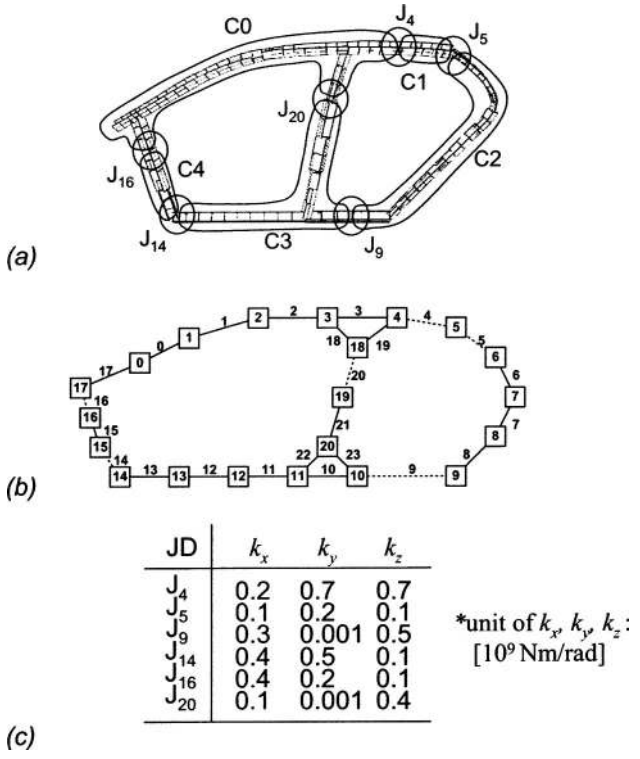

Fig. 18 Design R4. (*a*) Five components, (*b*) structural topology graph, and (*c*) joint designs.

Table 3 Objective function values for R1–R4

	$f_{stiffness}$ (mm)	$f_{manufac}$	$f_{assemble}$ (10^{*6} Nm/rad)
R1	−0.852	−5.573	−12.8
R2	−1.233	−4.477	−14.2
R3	−1.063	−6.878	0.0
R4	−0.919	−5.201	−10.0

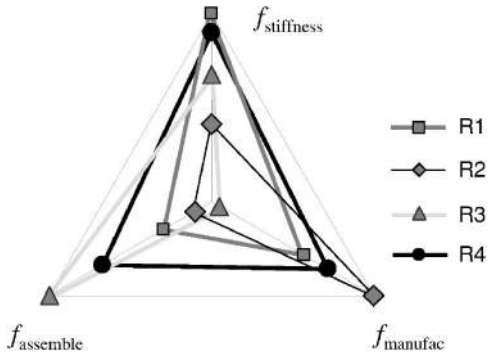

Fig. 19 Spider diagram of the four representative designs from the Pareto front in case study I, normalized within these four designs. Design R1, R2, and R3 show the best results only considering $f_{stiffness}$ value, $f_{manufac}$ value, and $f_{assemble}$ value, respectively. Design R4 shows balanced results in all three objective functions.

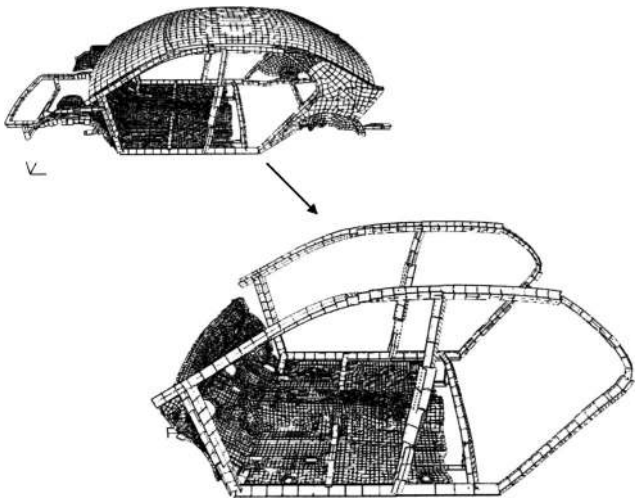

Fig. 20 Side/floor frame and floor panel in BIW model used in case study II

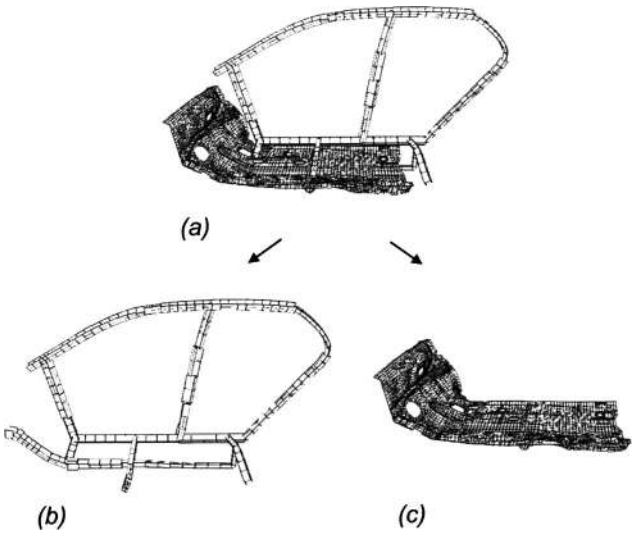

Fig. 21 (a) Entire structure to be decomposed (right half only), (*b*) beam substructure, and (*c*) plate substructure

rotations are parallel to the three axes in the global Cartesian coordinate system where x, y, and z directions are aligned along the length, width, and height of the car model.

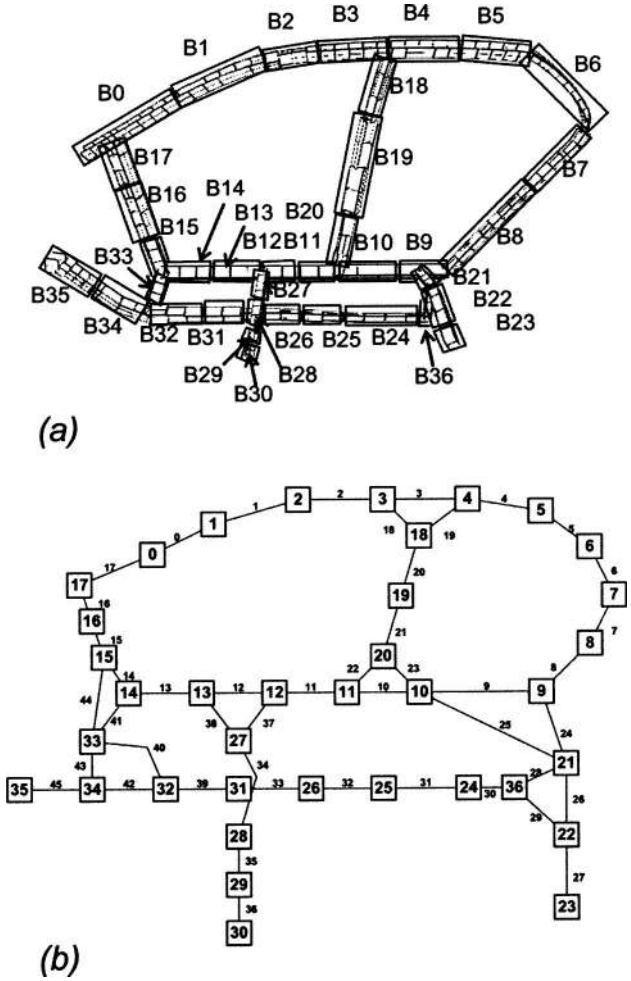

Fig. 22 (*a*) 37 basic members in beam substructure and (*b*) corresponding structural topology graph G_B with 37 nodes and 46 edges

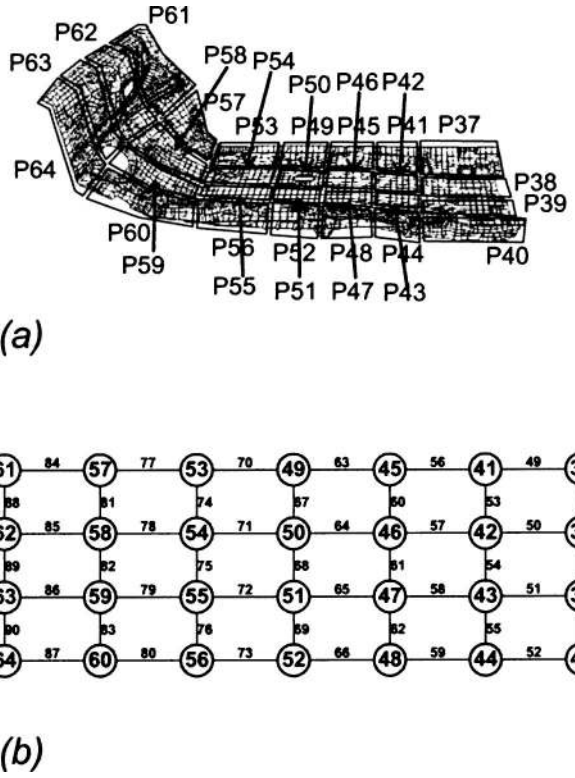

Fig. 23 (*a*) 28 basic members in plate substructure and (*b*) corresponding structural topology graph G_P with 28 nodes and 45 edges

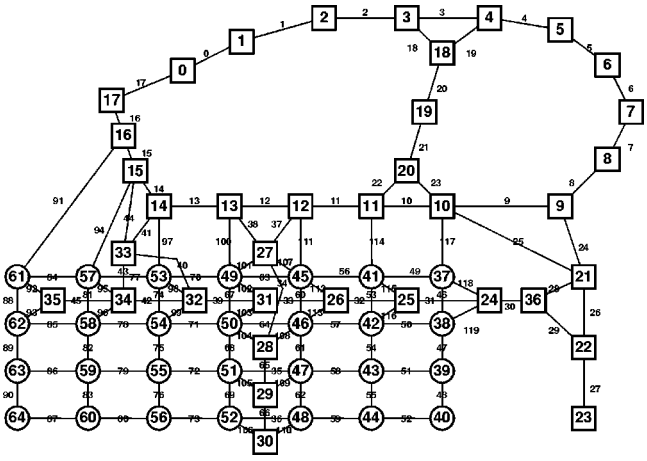

Fig. 24 Entire structural graph G_E with 65 nodes and 120 edges. In G_E, 29 edges (edge 91–edge 119) are used to connect beam basic member and plate basic member.

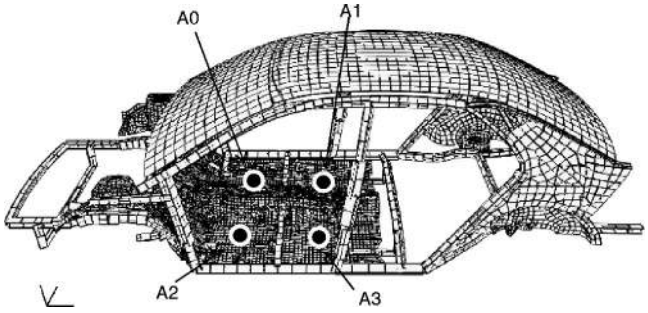

Fig. 25 Points for measuring deflection of floor panel

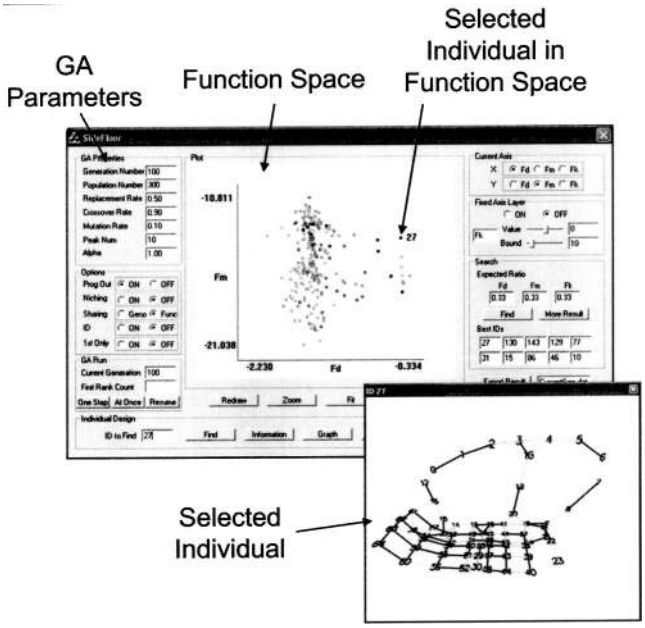

Fig. 26 GUI of the optimization software used in case study II

4.1 Case Study I: Side Frame. Figure 11(*a*) shows the side frame portion of the BIW model to be decomposed, which consists of beam elements. Using the symmetry, 21 basic members (Fig. 11(*b*)) were selected from one side frame. Figure 11(*c*) shows corresponding entire structural graph GE with 21 nodes and 24 edges, which is identical GB since there are only beam elements.

Under any loading conditions, the front door frame should retain its original shape with minimal distortion to guarantee the normal door opening and closing. In this case study, the stiffness function estimates the distortion of the deformed front door frame. Original (Fig. 12(*a*)) and deformed front door frame profile (Fig. 12(*b*)) are placed on each other for the hinge points (H0 and H1 in Fig. 12(*c*) to keep minimum distances (Fig. 12(*c*)). Distortion of the deformed front door frame is calculated by measuring the distances between prespecified points in the original front door frame profile and corresponding points in the deformed front door frame profile. Based on this consideration, DISPLACEMENTS function that determines $f_{\text{stiffness}}$ in Eq. (6) is defined as

$$\text{DISPLACEMENTS}(G_B(\mathbf{x}_B),\ G_P(\mathbf{x}_P),\mathbf{y}_B,\mathbf{y}_P,\mathbf{y}_{BP}) = \max_{i\in\{0,1,2,3\}} (\overline{AiBi}), \tag{8}$$

where Ai and Bi ($i=0,\ldots,3$) are location of a point in the front door frame before and after deformation, respectively.

Figure 13 shows GUI of the developed software for case study I showing the Pareto solutions at the terminal generation (100). Because there are three objective functions $f_{\text{stiffness}}$, f_{manufac}, and f_{assemble}, the resulting three-dimensional function space is projected on to three two-dimensional spaces as shown in Figs. 14(*a*)–14(*c*). Each 2D plot shows points for all 300 structural designs with respect to the chosen two objectives only, ignoring the values of the remaining one objective. In all plots, the utopia points are located at the upper right corner. The following observations are made on these Pareto graphs:

Observation 1: In $f_{\text{stiffness}}-f_{\text{manufac}}$ space (Fig. 14(*a*)), optimized designs are concentrated on the right upper corner.

Possible explanation: Lower stiffness (with more deflection) designs are usually composed of large number of small-sized components, which tends to show higher manufacturability.

Observation 2: In $f_{\text{stiffness}}-f_{\text{assemble}}$ space (Fig. 14(*b*)), optimized designs are not distributed on the upper-left corner.

Possible explanation: Lower stiffness (with more deflection) designs are usually composed of large number of components which requires large number of joints. As number of joints increases, total assembly cost also increases.

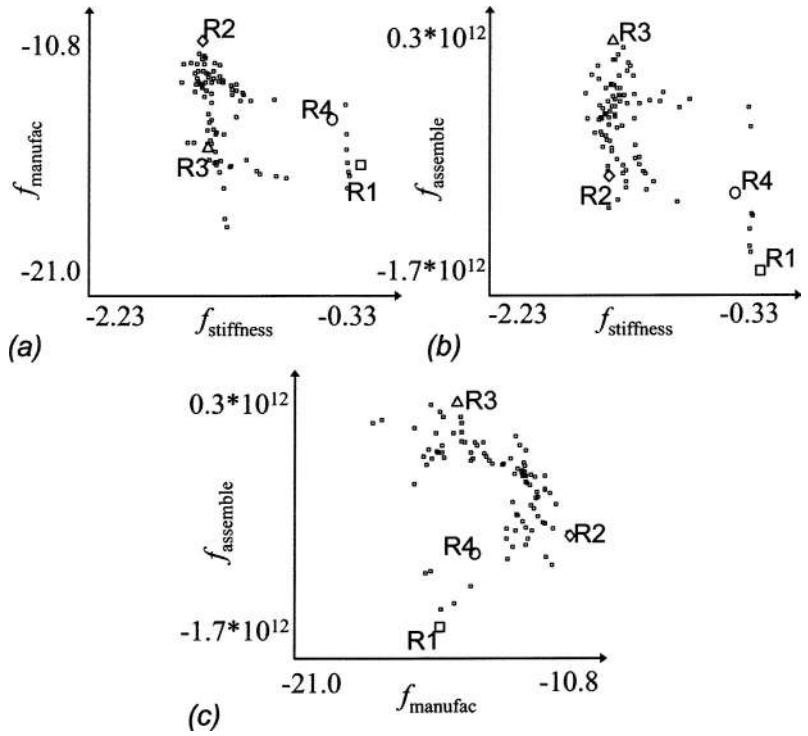

Fig. 27 Function values at the terminal generation (generation number=100). Points in the plots are the Pareto optimal designs.

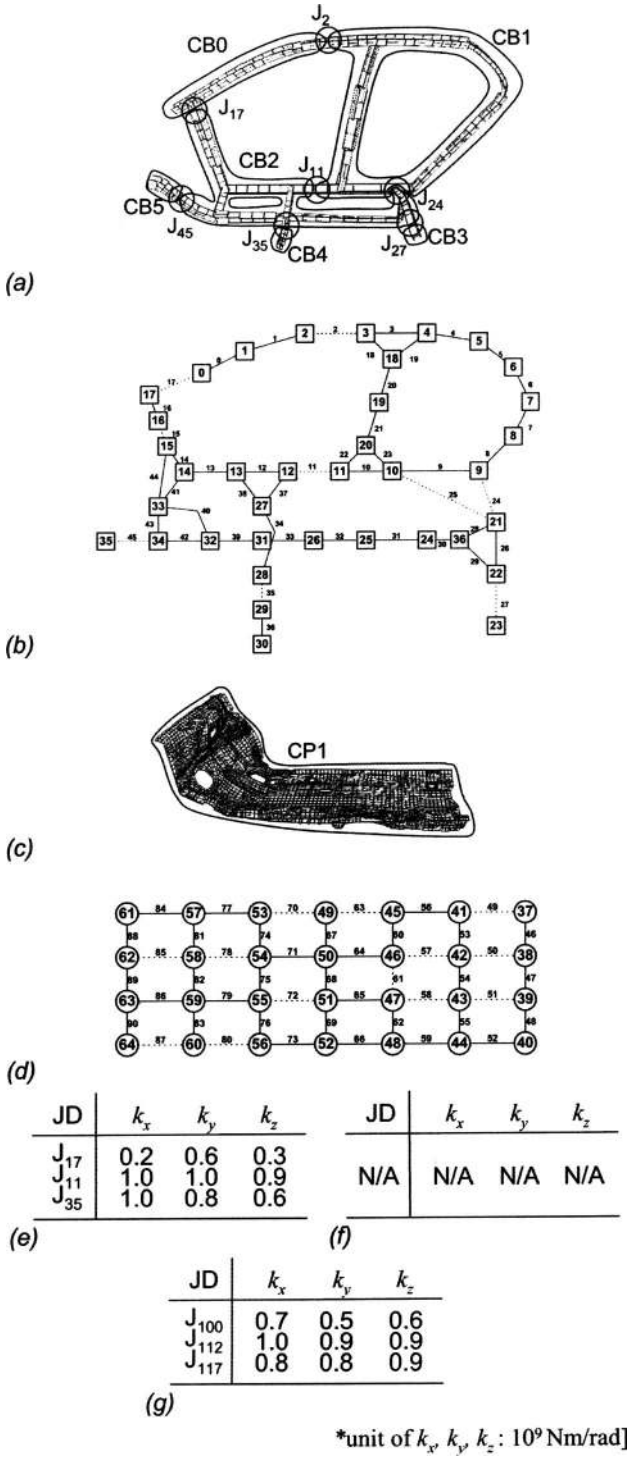

Fig. 28 Design R1 (best $f_{stiffness}$) (*a*) Six components in beam substructure, (*b*) G_B, (*c*) one component in plate substructure, (*d*) G_P, (*e*) joint designs (selected from seven joints) in beam substructure, (*f*) joint designs in plate substructure: not available (no joints), and (*g*) joint designs (selected from 29 joints) between beam and plate substructures

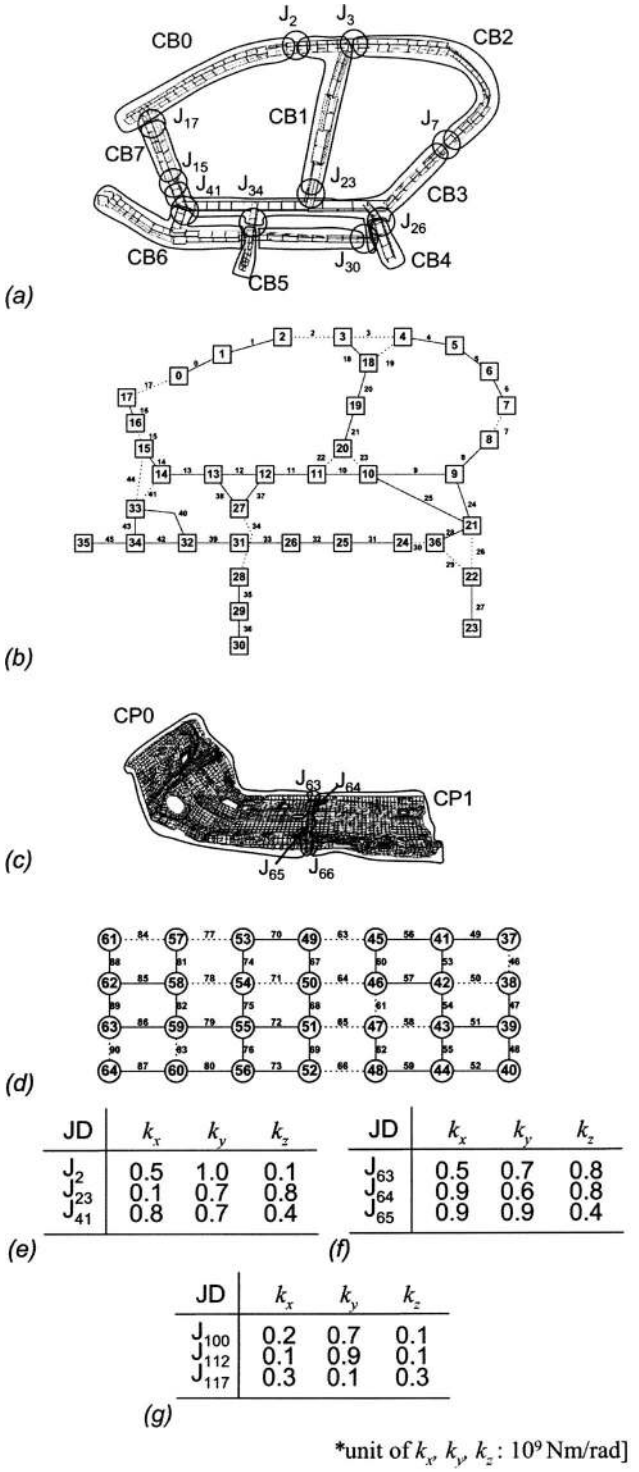

Fig. 29 Design R2 (best $f_{manufac}$). (*a*) Eight components in beam substructure, (*b*) G_B, (*c*) two components in plate structure, (*d*) G_P, (*e*) three joint designs (selected from 10 joints) in beam substructure, (*f*) three joint designs (selected from four joints) in plate substructure, (*g*) three joint designs (selected from 29 joints) between beam and plate structures.

Observation 3: In $f_{manufac}-f_{assemble}$ space (Fig. 14(*c*)), optimized designs with high manufacturing cost (low value of $f_{manufac}$) shows high value of $f_{assemble}$.

Possible explanation: Designs with high manufacturing cost tends to have small number of big-sized component, which requires small number of joints. Therefore, the cost of assembly is relatively low.

Four representative designs (R1–R4) are selected from the Pareto front and each design is illustrated in Figs. 15–18. Table 3 shows their objective function values and the following observations are made on these designs.

Design R1 (Fig. 15) shows the best design considering only $f_{stiffness}$ with four components that preserves the front door frame

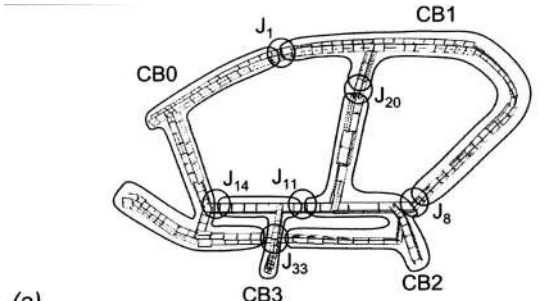

(a)

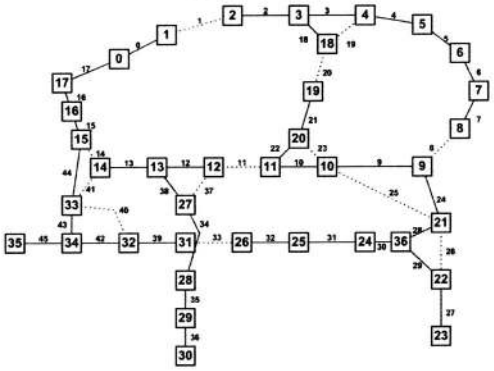

(b)

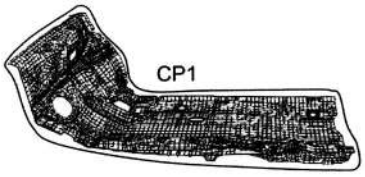

(c)

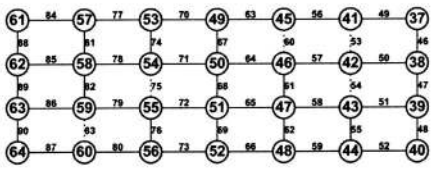

(d)

JD	k_x	k_y	k_z
J_1	0.6	0.3	0.2
J_{20}	0.3	0.2	0.4
J_{33}	0.5	0.4	0.001

(e)

JD	k_x	k_y	k_z
N/A	N/A	N/A	N/A

(f)

JD	k_x	k_y	k_z
J_{100}	0.001	0.3	0.2
J_{112}	0.5	0.2	0.2
J_{117}	0.3	0.001	0.001

(g)

*unit of k_x, k_y, k_z: 10^9 Nm/rad]

Fig. 30 Design R3 (best $f_{assemble}$). (*a*) Four components in beam substructure, (*b*) G_B, (*c*) one component in plate substructure, (*d*) G_P, (*e*) three joint designs (selected from six joints) in beam substructure, (*f*) joint designs in plate substructure: not available (no joints), (*g*) three joint designs (selected from 29 joints) between beam and plate structures.

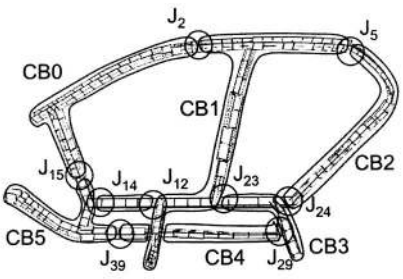

(a)

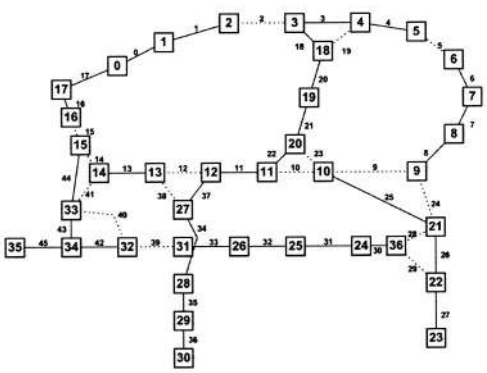

(b)

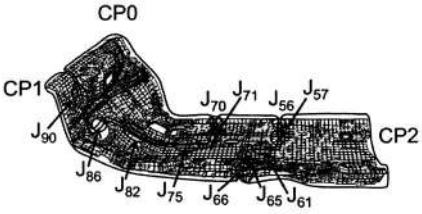

(c)

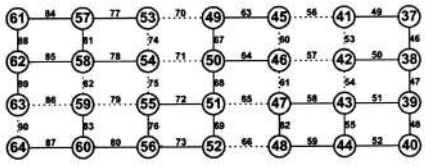

(d)

JD	k_x	k_y	k_z
J_{12}	0.1	0.9	0.001
J_{15}	0.001	0.5	0.3
J_{39}	0.001	0.3	0.4

(e)

JD	k_x	k_y	k_z
J_{57}	0.4	0.2	0.6
J_{71}	0.9	0.3	0.7
J_{90}	0.9	1.0	0.6

(f)

JD	k_x	k_y	k_z
J_{100}	0.1	0.4	0.001
J_{112}	0.2	1.0	0.3
J_{117}	0.2	0.3	0.3

(g)

*unit of k_x, k_y, k_z: 10^9 Nm/rad]

Fig. 31 Design R4. (*a*) Seven components in beam substructure, (*b*) G_B, (*c*) three components in plate substructure, (*d*) G_P, (*e*) three joint designs (selected from nine joints) in beam substructure, (*f*) three joint designs (selected from 11 joints) in plate substructure, and (*g*) three joint designs (selected from 29 joints) between beam and plate structures.

shape most close to the original front door frame shape by having no joints between the B-Pillar and the connecting positions of Roof Rail and Rocker Rail. Rear door frames includes three joints with small value of torsional spring rates allowing the rear door frame to absorb most distortion and leave the front door frame relatively undistorted.

Design R2 (Fig. 16) shows the best design considering only $f_{manufac}$. This six component design shows the best manufacturability by having all components in linear shape which minimizes the die usable area.

Design R3 (Fig. 17) shows the best design considering only $f_{assemble}$. It is composed of only one component, which eliminated

Table 4 Objective function values for R1–R4

	$f_{\text{stiffness}}$ (mm)	f_{manufac}	f_{assemble} (10^9 Nm/rad)
R1	−0.333	−16.311	−1.683
R2	−1.543	−10.811	−1.084
R3	−1.427	−16.671	−0.308
R4	−0.534	−14.711	−1.192

the joint in the structure, resulting minimum cost of assembly. Note this design is not best for $f_{\text{stiffness}}$, since this total rigid design without a compliant rear door frame causes more distortion in the front door frame than R1.

Design R4 (Fig. 18) shows the design considering all three objectives. Similar to R1, this five component design preserves the front door frame shape relatively undistorted by having no joints between the B-Pillar and Roof Rail/Rocker Rail. Also, all five components are relatively in linear shape to minimize the die usable area, which decide the total cost of manufacturing. As the Spider diagram in Fig. 19 indicates, it is the most balanced design in all three objectives.

4.2 Case Study II: Side/Floor Frame and Floor Panel Figure 20 shows the side frames, floor frames and floor panel in the BIW model, composed of beam elements (CBEAM) and plate elements (CQUAD4 and CTRIA3). The half structure (Fig. 21(*a*)) is divided into beam (Fig. 21(*b*)) and plate (Fig. 21(*c*)) substructures. Total of 37 basic members and 28 basic members are defined on beam and plate substructures, as in Fig. 22 and Fig. 23, respectively, with corresponding structural topology graphs G_B and G_P. Graph G_B is made of 37 nodes and 46 edges and G_P is made of 28 nodes and 45 edges. The entire structural graph G_E is illustrated in Fig. 24. It contains a total of 65 nodes and 120 edges, where 29 edges (edge 91–edge 119) are used to connect between beam and plate basic members.

In this case study, the maximum downward deflection of the four points on the floor panel in Fig. 25 is used in DISPLACEMENTS function:

$$\text{DISPLACEMENTS}(G_B(\mathbf{x}_B), G_P(\mathbf{x}_P), \mathbf{y}_B, \mathbf{y}_P, \mathbf{y}_{BP}) = \max_{i \in \{0,1,2,3\}} \text{deflection}(Ai), \quad (9)$$

where deflection(Ai) is the downward deflection at point Ai.

Figure 26 illustrates GUI of the developed software and the objective function values obtained at the terminal generation (=100) are illustrated in Fig. 27. As in case study I, each 2D plot shows the points in the 3D Pareto front with respect to the chosen two objectives only, ignoring the values of the remaining one objective. In all plots, the utopia points are located at the upper right corner. The following observation is made on these Pareto graphs:

Observation 1: In $f_{\text{manufac}} - f_{\text{assemble}}$ space (Fig. 27(*c*)), optimized designs with high manufacturing cost (low value of f_{manufac}) shows high value of f_{assemble}.

Possible explanation: Designs with high manufacturing costs tend to have small numbers of big-sized components, which requires a small number of joints. Therefore, the cost of assembly is relatively low.

Four representative designs (R1–R4) are selected from the Pareto front and each design is illustrated in Figs. 28–31. Table 4 shows their objective function values and the following observations are made on these designs.

Design R1 (Fig. 28) shows the best design considering only $f_{\text{stiffness}}$ with a big size floor frame component (CB2) and one piece panel component (CP1), which helped increase entire structural rigidity. However, by having one piece floor panel component sacrificed total manufacturability compared with the other three designs as shown in Fig. 32.

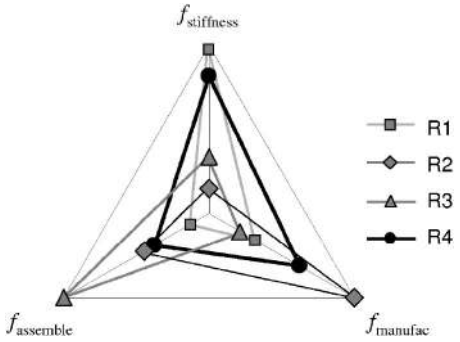

Fig. 32 Spider diagram of the four representative designs from the Pareto front in case study II, normalized within these four designs. Design R4 shows balanced results in all three objective functions.

Design R2 (Fig. 29) shows the best design considering only f_{manufac}. It contains eight beam components whose shapes are relatively linear which minimizes the die usable area for each component. However, by having more number of joints in the beam structure, this design shows the worst floor deflection compared with the other three designs.

Design R3 (Fig. 30) shows the best design considering only f_{assemble}. It contains one piece floor panel component which minimizes the use of joints in the floor panel and also minimizes the assembly cost. In the beam structure, it contains a relatively small number of components (four) and joints (Figs. 30(*e*)–30(g)) have smaller torsional spring rates. Smaller torsional spring rates indicate smaller number of spot welds, which also reduces the assembly cost. As in R1, by having one piece floor panel component, total manufacturability of structure was sacrificed compared with the other three designs.

Design R4 (Fig. 31) shows the design considering all three objectives. This design achieves relatively small floor panel deflection by component CB6 (Fig. 31(*a*)) containing one of the loading points. Having the loading point isolated in a small component seems to localize the effect of loading, resulting in small value of deflection. All seven beam components are in linear shape, which minimized the manufacturability. The Spider diagram in Fig. 19 indicates that design R4 is balanced in all three objectives compared with the other three designs.

5 Summary and Future Work

This paper described a method for synthesizing multicomponent structural assemblies, where the three-dimensional finite element model of a vehicle body-in-white (BIW) is optimally decomposed into a set of components considering the stiffness of the assembled structure under given loading conditions, as well as the manufacturability and assembleability of components. Multiobjective genetic algorithm combined with graph-based crossover and FEM analyses was used to obtain Pareto optimal solutions for the three objectives. Two case studies on 3D BIW model were presented to demonstrate the effectiveness of the proposed method. In the first case study, where side frame of BIW is decomposed for the minimum distortion of front door frame geometry under global bending, original front door frame shape could be preserved with little distortion by having no joints between the B-Pillar and the connecting positions of Roof Rail and Rocker Rail. In the second case study, where side/floor frame and floor panels are decomposed for the minimum floor deflections under global bending, designs with less number of joints in the floor panel showed less deflection in the floor panel. Also, designs with simpler com-

ponents shapes showed lower total manufacturing costs and designs with less number of joints showed lower total assembly costs.

For the future work of this research, other methods of manufacturing and assembly cost estimation will be implemented besides sheet metal working and spot welding procedures used in this paper. Also, the current method can only suggest the structural properties of joints between components. Methods of correlating suggested joint properties with real joint design will be also considered.

Acknowledgments

The authors acknowledge funding provided by Toyota Motor Corporation and National Science Foundation under CAREER Award (DMI-9984606) for this research. Any opinions, findings, and conclusions or recommendations expressed in this material are those of the authors and do not necessarily reflect the views of the National Science Foundation.

References

[1] Yetis, A., and Saitou, K., 2002, "Decomposition-Based Assembly Synthesis Based on Structural Considerations," ASME J. Mech. Des., **124**, pp. 593–601.
[2] Lee, B., and Saitou, K., 2003, "Decomposition-Based Assembly Synthesis for In-Process Dimensional Adjustability," ASME J. Mech. Des., **125**, pp. 464–473.
[3] Lyu, N., and Saitou, K., 2002, "Decomposition-Based Assembly Synthesis for Structural Stiffness," ASME J. Mech. Des., **125**, pp. 452–463.
[4] Fonseca, C. M., and Fleming, P. J., 1993, "Genetic Algorithms for Multiobjective Optimization: Formulation, Discussion and Generalization," *Proceedings of the Fifth International Conference on Genetic Algorithms*, San Mateo, California, pp. 416–423.
[5] Coello, C. A., Veldhuizen, D. A., and Lamont, G. B., 2002, *Evolutionary Algorithms For Solving Multiobjective Problems*, Kluwer Academic/Plenum, New York, p. 72.
[6] Laszewski, G., 1991, "Intelligent Structural Operators for the k-Way Graph Partitioning Problem," *Fourth International Conference on Genetic Algorithms*, pp. 45–52.
[7] Pereira, F., Machado, P., Costa, E., and Cardoso, A., 1999, "Graph Based Crossover—A Case Study With the Busy Beaver Problem," *Proceedings of the 1999 Genetic and Evolutionary Computation Conference*.
[8] Boothroyd, G., and Dewhurst, P., 1983, *Design for Assembly Handbook*, Univ. of Massachusetts, Amherst.
[9] Boothroyd, G., Dewhurst, P., and Knight, W., 1994, *Product Design for Manufacturing and Assembly*, Marcel Dekker, New York.
[10] Gupta, S. K., Regli, W. C., and Nau, D. S., 1994, "Integrating DFM With CAD Through Design Critiquing," Concurrent Engineering: Research and Application, **2**, pp. 85–95.
[11] Ashley, S., 1997, "Steel Cars Face a Weighty Decision," AMD (Am. Soc. Mech. Eng.), **119**, pp. 56–61.
[12] Barone, M. R. et al., 1981, *Modern Automotive Structural Analysis*, M. M. Kamal and J. A. Wolf, Jr., eds., Van Nostrand Reinhold Co., New York.
[13] Kirioka, K., 1966, "An Analysis of Body Structures," SAE Trans., **74**, pp. 164–190.
[14] Brown, J. C. et al., 2002, *Motor Vehicle Structures: Concept and Fundamentals*, SAE International, Butterworth-Heinemann, Woburn, MA..
[15] Chang, D., 1974, "Effects of Flexible Connections on Body Structural Response," SAE Trans., **83**, pp. 233–244.
[16] Garro, L., and Vullo, V., 1986, "Deformations Car Body Joints Under Operating Conditions," SAE Trans., **86**, pp. 5403–5420.
[17] Lee, K., and Nikolaidis, E., 1992, "A Two-Dimensional Model for Joints in Vehicle Structures," Comput. Struct., **45**, pp. 775–784.
[18] Lee, K., and Nikolaidis, E., 1998, "Effect of Member Length on the Parameter Estimates of Joints," Comput. Struct., **68**, pp. 381–391.
[19] Long, L., 1998, "Design-Oriented Translators for Automotive Joints," PhD. Thesis, Virginia Polytechnic Institute.
[20] Kim, J., Kim, H., Kim, D., and Kim, Y., 2002, "New Accurate Efficient Modeling Techniques for the Vibration Analysis of T-Joint Thin-Walled Box Structures," Int. J. Solids Struct., **39**, pp. 2893–2909.
[21] Coello, C. A., Veldhuizen, D. A., and Lamont, G. B., 2002, *Evolutionary Algorithms for Solving Multiobjective Problems*, Kluwer Academic/Plenum, New York.
[22] Fonseca, C. M., and Fleming, P. J., 1993, "Genetic Algorithms for Multiobjective Optimization: Formulation, Discussion and Generalization," *Proceedings of the Fifth International Conference on Genetic Algorithms*, pp. 416–423.
[23] Srinivas, N., and Deb, K., 1994, "Multiobjective Optimization Using Nondominated Sorting in Genetic Algorithms," Evol. Comput., **2**, pp. 221–248.
[24] Deb., K., Agrawal, S., Pratab, A., and Meyarivan, T., 2000, "A Fast Elitist Non-Dominated Sorting Genetic Algorithm for Multi-Objective Optimization: NSGA-II," *KanGAL report 200001*, Indian Institute of Technology, Kanpur, India.
[25] Horn, J., Nafpliotis, N., and Goldberg, D. E., 1994, "A Niched Pareto Genetic Algorithm for Multiobjective Optimization," *Proceedings of the First IEEE Conference on Evolutionary Computation, IEEE World Congress on Computational Intelligence*, Vol. 1, pp. 82–87.
[26] Goldberg, D. E., 1989, *Genetic Algorithms in Search, Optimization and Machine Learning*, Addison-Wesley, Massachusetts.
[27] Zitzler, E., and Thiele, L., 1998, "An Evolutionary Algorithm for Multiobjective Optimization: The Strength Pareto Approach," *Technical Report 43*, Computer Engineering and Communication Networks Lab, Swiss Federal Institute of Technology, Zurich, Switzerland.
[28] Knowles, J. D., and Corne, D. W., 1999, "The Pareto Archived Evolution Strategy: A New Baseline Algorithm for Multiobjective Optimization," *1999 Congress on Evolutionary Computation*, Washington, DC, pp. 98–105.
[29] Garey, M. R., and Johnson, D. S., 1979, *Computers and Intractability, a Guide to the Theory of NP-Completeness*, W. H. Freeman, New York.
[30] Lyu, N., and Saitou, K., 2003, "Topology Optimization of Multi-Component Structures Via Decomposition-Based Assembly Synthesis," *Proceedings of the 2003 ASME DETC*, September 2–6, 2003, Chicago, IL, DETC2003/DAC-48730.